Journal of Materials Chemistry B

ROYAL SOCIETY OF CHEMISTRY

PAPER

View Article Online
View Journal | View Issue

Cite this: J. Mater. Chem. B, 2025, 13, 599

Development of a diagnostic and drug evaluation system for acute inflammation using a novel [^{89}Zr]DTPA-sorbitol probe†

Seung Ho Baek,[ac] Eun-Ha Hwang,[a] Sang Bong Lee,[de] Miji Kim,[a] Dong-Yeon Kim,[a] Jung Joo Hong *[ab] and Kyung-Sun Kang*[c]

Received 12th September 2024,
Accepted 18th November 2024

DOI: 10.1039/d4tb02061h

rsc.li/materials-b

Non-invasive imaging techniques employing biomarkers with high selectivity for inflammation are essential not only for the early diagnosis and prevention of chronic inflammatory diseases but also for guiding appropriate drug therapy and enabling real-time evaluation of anti-inflammatory drug efficacy. In this study, we conjugated radioactive zirconium to sorbitol, a compound that can selectively target inflammation, and evaluated its inflammation-specific uptake and potential for assessing anti-inflammatory treatment efficacy in a mouse inflammation model. Pharmacokinetic analysis demonstrated that radiolabeled sorbitol achieved maximal uptake in inflamed tissues within 1 h. Positron emission tomography imaging further confirmed its utility in monitoring therapeutic effects during anti-inflammatory drug treatment. Our findings suggest that [^{89}Zr]DTPA-sorbitol is a promising radioprobe for targeting rapid systemic inflammation, particularly in tissues demonstrating minimal non-specific uptake, such as the brain, heart, and lung tissues. Additionally, it holds significant potential for the *in vivo* evaluation of anti-inflammatory drug efficacy.

Introduction

Inflammation is a crucial immune response in the human body, essential for eliminating external invaders such as bacteria, viruses, noxious stimuli, and injury, as well as for repairing damaged tissue.[1–4] These inflammatory reactions are initiated during innate immune responses through the recognition of pathogen-associated molecular patterns and damage-associated molecular patterns.[5–9] They are subsequently triggered by cytokines produced by dendritic cells, macrophages, and other immune cells, and are further refined and sustained during adaptive immune responses.[1,10–12] While host inflammatory responses are vital, repetitive or abnormal inflammatory reactions are closely associated with chronic diseases, including cardiovascular diseases, rheumatoid arthritis, inflammatory diabetes, chronic respiratory diseases, Alzheimer's disease, and cancer.[13,14] Conventional hematological assays, such as C-reactive protein and erythrocyte sedimentation rate tests, although proficient in indicating the presence of systemic inflammation, typically require several days for results processing.[15–17] Moreover, these assays lack the capability to localize the site and extent of inflammatory activity within the body and fail to provide rapid feedback. Early diagnosis of the extent and precise location of inflammation is crucial not only for the timely application of pharmacological interventions and the development of treatment strategies but also for improving patient outcome.

Inflammation targeting typically employs small molecules, antibodies, and peptides that interact with cell membrane receptors or bind to receptors activated by inflammation.[18–20] Gadolinium, commonly used in magnetic resonance imaging for inflammation, suffers from low sensitivity. This limitation is addressed by encapsulating gadolinium within dendrimers, micelles, or nanoparticles to enhance MRI sensitivity.[21,22] However, the toxicity of gadolinium presents challenges for MRI-based inflammation imaging. Fluorescent imaging probes are also affected by light scattering and tissue attenuation, impacting penetration depth and making anatomical matching difficult, thus limiting the localization and quantitative analysis of inflammation.[23,24] In contrast, positron emission tomography (PET) imaging is highly suitable for inflammation imaging due to its superior penetration, high sensitivity.[25,26] Examples of radioactive-labeled probes include 2-[^{18}F]-fluorodeoxyglucose

[a] National Primate Research Center, Korea Research Institute of Bioscience and Biotechnology, Cheongju 28116, Republic of Korea. E-mail: hong75@kribb.re.kr
[b] KRIBB School of Bioscience, Korea University of Science & Technology (UST), Daejeon 34113, Republic of Korea
[c] Department of Veterinary Public Health, College of Veterinary Medicine, Seoul National University, Seoul 08826, Republic of Korea
[d] SimVista, A-13, 194-25, Osongsaengmueong1-ro, Osong-eup, Heungdeok-gu, Cheongju-si, Chungcheongbuk-do, Republic of Korea
[e] Department of Biomedical Sciences, Chonnam National University Medical School, Gwangju 61469, South Korea

† Electronic supplementary information (ESI) available. See DOI: https://doi.org/10.1039/d4tb02061h

([^{18}F]FDG), which enters cells *via* type-1 and type-3 glucose transporters exploiting glucose metabolism, while [^{68}Ga]DOTA-TATE targets inflammation by binding to somatostatin receptors.[27–30] However, the nonspecific uptake of these radiotracers complicates and hampers the interpretation of inflammation imaging. Additionally, their short half-lives render them unsuitable for long-term inflammation monitoring.

Sorbitol, a sugar alcohol is widely used as a metabolic substrate in food, beverages, and pharmaceuticals. It can be synthesized through the reduction of glucose, wherein the aldehyde group is converted into a hydroxyl group with a different orientation at carbon 2. Given that sorbitol is a glucose derivative with a similar structure, we hypothesized that it could potentially be used to target inflammation. In this study, we stably labeled sorbitol with ^{89}Zr using a diethylenetriaminepentaacetic acid (DTPA) chelator and analyzed its selectivity for inflamed tissues, compared with that of [^{18}F]FDG, in a mouse inflammation model. In the present study, we aim to evaluate the utility of zirconium-labeled sorbitol in diagnosing inflammation and explore its potential as a method for evaluating anti-inflammatory drugs.

Experimental section

DTPA-sorbitol conjugation

Detailed procedures for the conjugation of DTPA-sorbitol are described in the ESI.†

Radiolabeling of zirconium-89

^{89}Zr labeling procedures and radio-TLC analysis are described in the ESI.†

PET/CT imaging

Study 1. For inflammation induction, PBS and 4% carrageenan (CG) were injected to the respective thighs. [^{89}Zr]DTPA-sorbitol (180 MBq kg^{-1}) were intravenously administered to animals after approximately 10 seconds of inhalation anaesthesia with isoflurane. PET/CT were performed at the indicated time points for [^{89}Zr]DTPA-sorbitol kinetics (3 mice) and at 1 h for targeting inflammatory lesion (n = 4).

Study 2. 9α-Fluoro-11β,17α,21-trihydroxy-16α-methylpregna-1,4-diene-3,20-dione (dexamethasone, DEX) (20 mg kg^{-1}) was administered intraperitoneally 10 minutes prior to CG and PBS administration. 6 h after inducing inflammation, [^{89}Zr]DTPA-sorbitol was injected *via* the tail vein with inhalation anaesthesia, and PET/CT scanning was performed 1 h post-injection (n = 4).

Study 3. [^{18}F]FDG were intravenously administered to animals with anaesthesia (n = 4). After 1 h, PET/CT scan was conducted and major organs were excised for gamma-counter measurement.

PET/CT imaging analysis

For PET/CT analysis, CT was performed for attenuation correction (480 projections, 50 kVp, 660 μA, 300 ms) followed by PET scans were conducted using the micro PET/CT system (Mediso Ltd, Hungary). PET images were obtained by Tera-Tomo 3D iterative reconstruction. PET images were co-registered with anatomical CT images using Siemens Inveon Research Workplace (IRW 2.0.0.1050).

Bio-distribution study

Mice (n = 4) were injected [^{89}Zr]DTPA-sorbitol (3.7 MBq) in the tail vein and sacrificed at the indicated times. After PET/CT scan, major organs were dissected, weighed and measured the radioactivity using a gamma counter (Hidex AMG, Turku, Finland). The results were calculated as % injected dose per gram of tissue (%ID per g).

Immunohistology

Immediately after biodistribution assay, left and right thigh muscles were fixed in 4% paraformaldehyde and embedded in paraffin, as described previously.[31] Briefly, four to five μm sections were stained with hematoxylin and eosin and examined microscopically for signs of inflammation.

Results and discussion

Synthesis and characterization of [^{89}Zr]DTPA-sorbitol

Amino-sorbitol was conjugated with NCS-DTPA through amide bond formation *via* a condensation reaction, resulting in a DTPA-sorbitol conjugate, which can be used to track inflammation *in vivo* using a real-time PET imaging system (Fig. 1). The DTPA-sorbitol conjugate was confirmed by ^{1}H and ^{13}C nuclear magnetic resonance, liquid chromatography-mass spectrometry, and high-performance liquid chromatography (Fig. S1 and S2, ESI†).

DTPA-sorbitol was conjugated with [^{89}Zr]oxalate in HEPES buffer at pH 7.4. To determine the optimal reaction time and stability, we analyzed the labeling efficiency over 60 min using radio-thin-layer-chromatography. Labeling using [^{89}Zr]DTPA-sorbitol was efficient, with a radiochemical yield of 87.51% achieved in just 10 min, reaching 99.24% at 50 min, with stability maintained for up to 72 h (Fig. 2 and Fig. S3, ESI†).

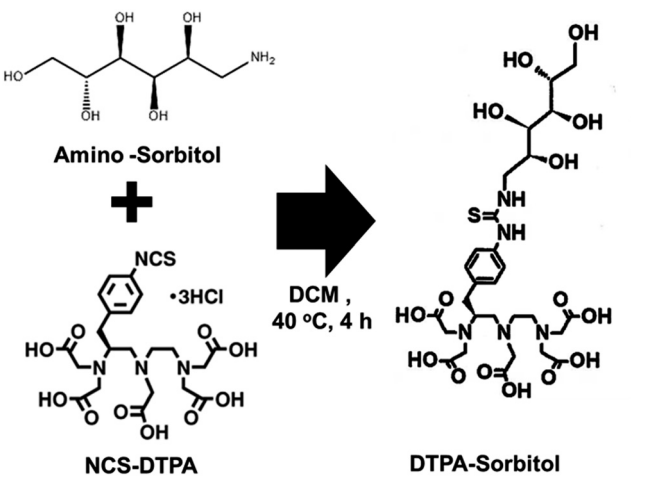

Fig. 1 Preparation of amino-sorbitol conjugated with NCS-DTPA.

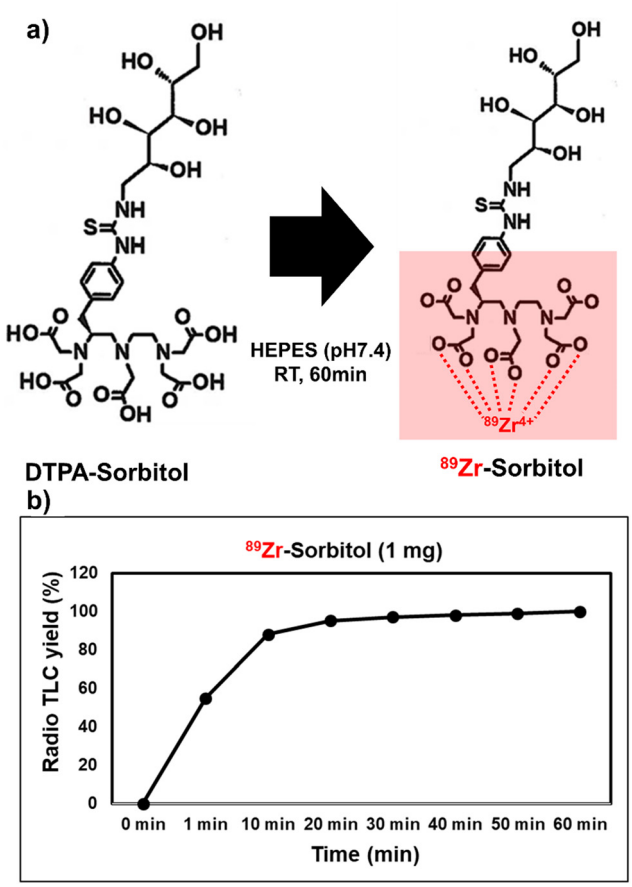

Fig. 2 (a) Radioactive zirconium conjugation with DTPA-sorbitol in HEPES buffer, pH 7.4, 36.5 °C. (b) Kinetic analysis of radiolabeled zirconium chelation with DTPA with radio-TLC.

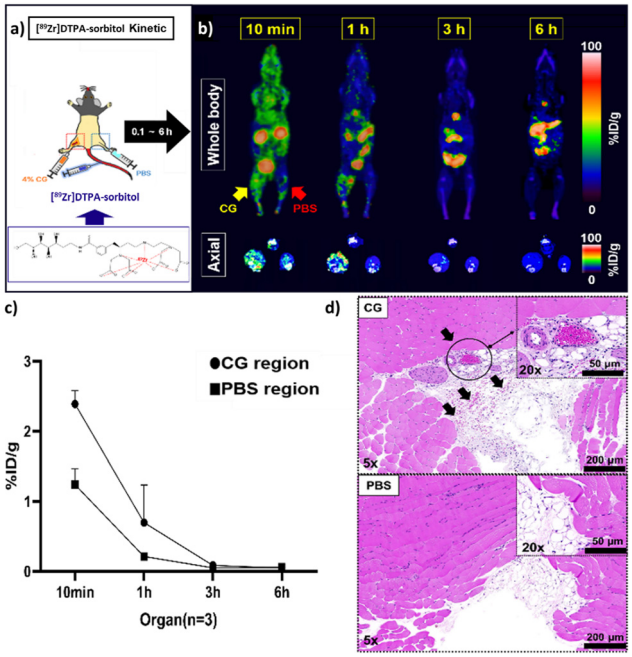

Fig. 3 PET kinetic imaging study by [^{89}Zr]DTPA-sorbitol. (a) and (b) The procedure for the [^{89}Zr]DTPA-sorbitol kinetic PET imaging and coronal (upper) and axial section (lower) combined PET-CT images of [^{89}Zr]DTPA-sorbitol (3.7 MBq) in carrageenan-induced inflammation mice recorded at 10 min, 1, 3, 6 hours after tail vein injection of [^{89}Zr]DTPA-sorbitol. (c) Region of interest (ROI) quantification results are shown as %ID per g of CG and PBS injected thigh after intravenous injection of [^{89}Zr]DTPA-sorbitol (n = 3). (d) Histological analysis of bilateral thigh tissues at 6 hours post-CG-induced inflammation.

Visualization of [^{89}Zr]DTPA-sorbitol uptake in acute inflammation sites by real-time PET/CT imaging

To evaluate the potential cytotoxicity of the synthesized DTPA-sorbitol for successful inflammation targeting, we conducted *in vitro* toxicity tests. The results showed no signs of cytotoxicity upon incubating the cells with various concentrations of DTPA-sorbitol (Fig. S4, ESI†). To assess the uptake of [^{89}Zr]DTPA-sorbitol in inflamed tissues, the radiolabelled probe was intravenously injected into mice (n = 4) with CG-induced inflammation. Histopathological analysis of both thigh tissues was performed 6 hours post-CG exposure, revealing a significant leukocyte infiltration in the inflamed tissue, while PBS-injected tissue exhibited normal histology (Fig. 3d). PET imaging conducted over a period of 10 minutes to 6 hours provided real-time visualization of systemic distribution and rapid accumulation of the radioprobe at inflammation sites, with subsequent renal and bladder excretion (Fig. 3a). Within 10 minutes post-injection, the radiolabeled sorbitol demonstrated rapid localization to the CG-induced inflammation site (left thigh), followed by systemic circulation and clearance *via* the kidneys and bladder. At 1 h post-injection, PET imaging confirmed a higher accumulation of sorbitol in the inflamed left thigh relative to the contralateral, PBS-injected control tissue, with additional uptake observed in the gallbladder, spleen, and intestines. Systemic clearance of the radioprobe was evident at 1 hour compared to the distribution observed at 10 minutes. By 3 hour post-injection, radiolabelled sorbitol had largely cleared from the inflammation site, with residual signals detected primarily in the gastrointestinal tract, persisting for up to 6 h (Fig. 3b). These results indicate that [^{89}Zr]DTPA-sorbitol rapidly and selectively accumulates in inflamed tissues shortly after administration, with peak uptake observed at 1 hour post-injection and low background signal, providing clear visualization of inflammatory regions (Fig. 3a).

Assessment of the effect of anti-inflammatory agents on [^{89}Zr]DTPA-sorbitol uptake in inflammatory lesion using established inflammation-targeting strategies

To validate the application of [^{89}Zr]DTPA-sorbitol PET imaging as a tool for assessing anti-inflammatory drugs, we compared the distribution of radioactive sorbitol in a CG-induced inflammation model and DEX-treated mice. Based on the PET kinetic imaging results (Fig. 4a), biodistribution analysis was conducted at 1 h (optimal inflammation targeting time) after the administration of radiolabeled sorbitol. In the [^{89}Zr]DTPA-sorbitol PET study, uptake in digestive organs and rapid renal excretion were consistent with those of those of previous kinetic studies (Fig. 3b). In contrast, [^{18}F]FDG was excreted through the kidneys more rapidly than sorbitol, yet showed

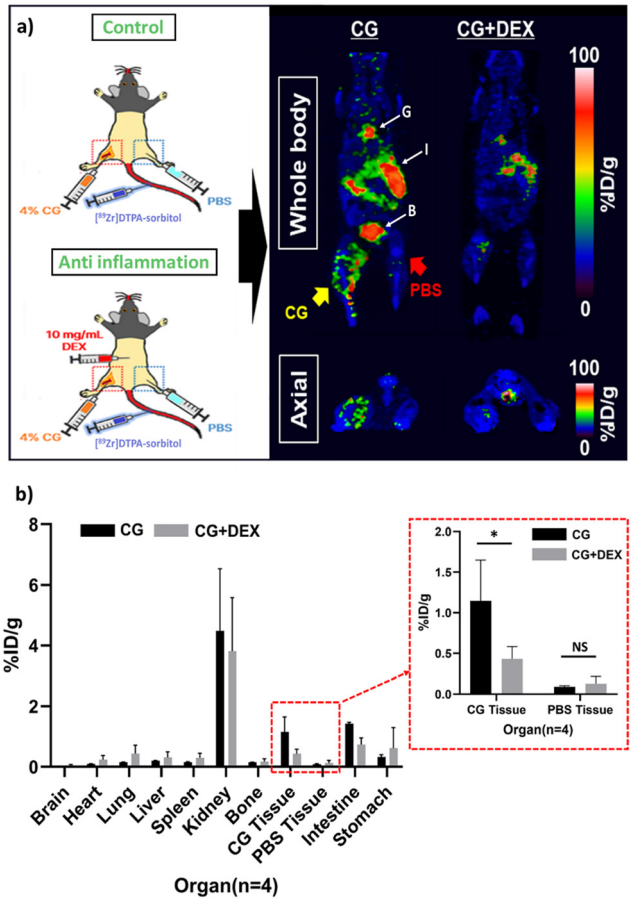

Fig. 4 *In vivo* study of [^{89}Zr]DTPA-sorbitol in CG-induced inflammation and anti-inflammatory treated mice. (a) PET images (axial, coronal sections) of a mouse injected with [^{89}Zr]DTPA-sorbitol. (b) Bio-distribution of major organs of inflammation and anti-inflammation models. G: gallbladder, I: intestines, B: bladder. CG: carrageenan, DEX: dexamethasone.

markedly higher uptake in the brain, heart, and lungs, as well as a tendency for elevated uptake in normal muscle tissues injected with PBS (Fig. S6a, ESI†). From an inflammation-targeting perspective, the percent injected dose per gram tissue (%ID per g) of [^{89}Zr]DTPA-sorbitol in inflammation-induced tissues was approximately 2.45 times higher than that of [^{18}F]FDG, whereas in PBS-injected tissues, [^{18}F]FDG was approximately 2.58 times higher. Importantly, sorbitol uptake was significantly lower in the inflammed sites treated with anti-inflammatory drugs compared to the solely inflamed tissue sites (Fig. 4b and Fig. S6b, ESI†).

The results of the hematoxylin & eosin staining, which was conducted simultaneously, also clearly demonstrate the induction of inflammation by CG and its inhibition by DEX (Fig. 5).

Conclusions

In this study, we have demonstrated inflammation-targeted imaging using PET imaging with radiolabeled sorbitol. We labeled sorbitol with zirconium-89 using a chelator and its specific uptake in CG-induced inflammation sites was demonstrated *in vivo*. Unlike high molecular weight antibody- or peptide-based radiotracers, this

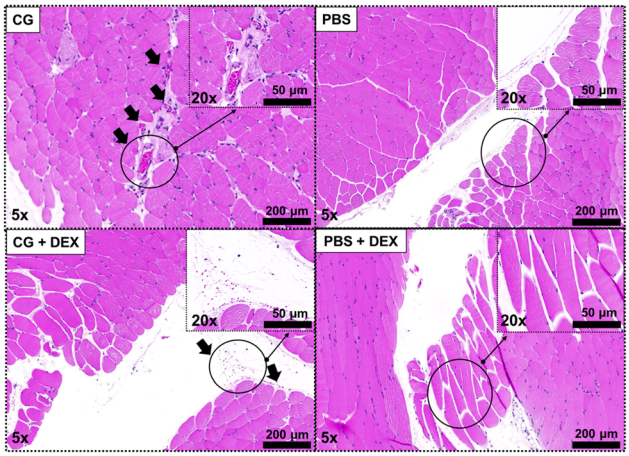

Fig. 5 Histological images from the thigh tissues of mice. Photograph of CG + DEX showing the inhibition effect of DEX against CG-induced inflammation.

compound avoided hepatic uptake and was rapidly excreted through the urinary system. Additionally, the potential of [^{89}Zr]DTPA-sorbitol as a method for evaluating the efficacy of anti-inflammatory treatments was effectively validated. Sorbitol was metabolized in inflamed tissues much faster than expected. Thus, sorbitol is expected to be used as an imaging probe for non-invasive assessment of various inflammatory conditions anti-inflammatory effects. Furthermore, the simple and rapid labeling procedure, along with excellent binding stability, enhances the reliability of experimental results and suggests potential applications in diagnosing inflammatory diseases in organs with minimal non-specific uptake such as the brain, lungs, heart, and liver. Further PET imaging studies on the application of this radiolabeled compound for cancer diagnosis and treatment are currently underway.

Author contributions

Seung Ho Baek: conceptualization, methodology, writing – original draft, Eun-Ha Hwang, Sang Bong Lee, Miji Kim, Dong-Yeon Kim: validation formal analysis, resource, Jung Joo Hong, and Kyung-Sun Kang: conceptualization, methodology, formal analysis, resources, funding acquisition, writing – review & editing, supervision.

Data availability

The datasets generated and analysed in the current study are available from the corresponding author on reasonable request.

Conflicts of interest

There are no conflicts to declare.

Acknowledgements

This work was supported by the Ministry of Science and ICT of Korea (Korea Research Institute of Bioscience and Biotechnology

Research Initiative Programs (grant number KGM 4572431) and the National Research Foundation of Korea (NRF) funded by Korea [A1] government (MSIP; grant number 2022R1F1A1063012). We thank the isotope production staff of the Korea Atomic Energy Research Institute (KAERI, Jeongeup, Korea)

References

1 Y. Belkaid and T. W. Hand, *Cell*, 2014, **157**, 121–141.
2 M. W. Hornef, M. J. Wick, M. Rhen and S. Normark, *Nat. Immunol.*, 2002, **3**, 1033–1040.
3 A. Osuka, H. Ogura, M. Ueyama, T. Shimazu and J. A. Lederer, *Acute Med. Surg.*, 2014, **1**, 63–69.
4 R. C. Sterner and R. M. Sterner, *Front. Immunol.*, 2022, **13**, 1084101.
5 R. A. Burgoyne, A. J. Fisher and L. A. Borthwick, *Cells*, 2021, **10**, 10.
6 A. Hassanshahi, M. Moradzad, S. Ghalamkari, M. Fadaei, A. J. Cowin and M. Hassanshahi, *Cells*, 2022, **11**, 19.
7 K. Moriyama and O. Nishida, *Int. J. Mol. Sci.*, 2021, **22**, 16.
8 C. Qian and X. Cao, *Semin. Immunol.*, 2018, **35**, 3–11.
9 J. S. Roh and D. H. Sohn, *Immune Network*, 2018, **18**, e27.
10 M. Chieppa, *Int. J. Mol. Sci.*, 2020, **21**, 12.
11 Y. Oishi and I. Manabe, *Int. Immunol.*, 2018, **30**, 511–528.
12 A. V. Sen'kova, I. A. Savin, E. L. Chernolovskaya, A. S. Davydova, M. I. Meschaninova, A. Bishani, M. A. Vorobyeva and M. A. Zenkova, *Acta Nat.*, 2024, **16**, 61–71.
13 D. Furman, J. Campisi, E. Verdin, P. Carrera-Bastos, S. Targ, C. Franceschi, L. Ferrucci, D. W. Gilroy, A. Fasano, G. W. Miller, A. H. Miller, A. Mantovani, C. M. Weyand, N. Barzilai, J. J. Goronzy, T. A. Rando, R. B. Effros, A. Lucia, N. Kleinstreuer and G. M. Slavich, *Nat. Med.*, 2019, **25**, 1822–1832.
14 A. B. Kunnumakkara, B. L. Sailo, K. Banik, C. Harsha, S. Prasad, S. C. Gupta, A. C. Bharti and B. B. Aggarwal, *J. Transl. Med.*, 2018, **16**, 14.
15 M. K. Litao and D. Kamat, *Pediatr. Ann.*, 2014, **43**, 417–420.
16 C. K. Orr, A. Najm, F. Young, T. McGarry, M. Biniecka, U. Fearon and D. J. Veale, *Front. Med.*, 2018, **5**, 185.
17 J. Watson, C. Salisbury, J. Banks, P. Whiting and W. Hamilton, *Br. J. Cancer*, 2019, **120**, 1045–1051.
18 A. Autio, T. Ujula, P. Luoto, S. Salomaki, S. Jalkanen and A. Roivainen, *Eur. J. Nucl. Med. Mol. Imaging*, 2010, **37**, 1918–1925.
19 S. Bhatnagar, E. Khera, J. Liao, V. Eniola, Y. Hu, D. E. Smith and G. M. Thurber, *Sci. Rep.*, 2019, **9**, 4661.
20 A. J. M. Lewis, J. J. Miller, A. Z. Lau, M. K. Curtis, O. J. Rider, R. P. Choudhury, S. Neubauer, C. H. Cunningham, C. A. Carr and D. J. Tyler, *Circ. Res.*, 2018, **122**, 1084–1093.
21 K. J. Chen, S. M. Wolahan, H. Wang, C. H. Hsu, H. W. Chang, A. Durazo, L. P. Hwang, M. A. Garcia, Z. K. Jiang, L. Wu, Y. Y. Lin and H. R. Tseng, *Biomaterials*, 2011, **32**, 2160–2165.
22 K. Luo, G. Liu, W. She, Q. Wang, G. Wang, B. He, H. Ai, Q. Gong, B. Song and Z. Gu, *Biomaterials*, 2011, **32**, 7951–7960.
23 J. Cao, B. Zhu, K. Zheng, S. He, L. Meng, J. Song and H. Yang, *Front. Bioeng. Biotechnol.*, 2019, **7**, 487.
24 S. Zhang, P. Shao, X. Ling, L. Yang, W. Hou, S. H. Thorne, W. Beaino, C. J. Anderson, Y. Ding and M. Bai, *Am. J. Nucl. Med. Mol. Imaging*, 2015, **5**, 246–258.
25 D. Gao, Y. Miao, S. Ye, C. Lu, G. Lv, K. Li, C. Yu, J. Lin and L. Qiu, *RSC Adv.*, 2021, **11**, 18738–18747.
26 A. Signore and A. W. Glaudemans, *Ann. Nucl. Med.*, 2011, **25**, 681–700.
27 M. Mamede, T. Higashi, M. Kitaichi, K. Ishizu, T. Ishimori, Y. Nakamoto, K. Yanagihara, M. Li, F. Tanaka, H. Wada, T. Manabe and T. Saga, *Neoplasia*, 2005, **7**, 369–379.
28 E. Puuvuori, F. Liggieri, I. Velikyan, E. Chiodaroli, J. Sigfridsson, H. Romelin, S. Ingvast, O. Korsgren, G. Hulsart-Billstrom, G. Perchiazzi and O. Eriksson, *EJNMMI Res.*, 2022, **12**, 19.
29 S. J. Raheem, A. K. Salih, M. D. Garcia, J. C. Sharpe, B. M. Toosi and E. W. Price, *Bioconjug. Chem.*, 2023, **34**, 549–561.
30 Z. G. Wang, M. M. Yu, Y. Han, F. Y. Wu, G. J. Yang, D. C. Li and S. M. Liu, *Medicine*, 2016, **95**, e5462.
31 G. Kim, D. H. Kim, H. Oh, S. Bae, J. Kwon, M. J. Kim, E. Lee, E. H. Hwang, H. Jung, B. S. Koo, S. H. Baek, P. Kang, Y. J. An, J. H. Park, J. H. Park, K. S. Lyoo, C. M. Ryu, S. H. Kim and J. J. Hong, *J. Infect. Dis.*, 2021, **224**, 1861–1872.